Comparing Aerodynamic Models for Numerical Simulation of Dynamics and Control of Aircraft

Christopher J. Sequeira* and David J. Willis*

Jaime Peraire†

Massachusetts Institute Of Technology, 77 Massachusetts Ave., Cambridge, MA 02139, USA.

Stability and control derivatives are routinely used in the design and simulation of aircraft, yet other aerodynamics models exist that can provide more accurate results for certain simulations without a large increase in computational time. In this paper, several aerodynamics models of varying fidelity are coupled with a six degrees of freedom rigid body dynamics simulation tool to model various geometries under a number of different initial conditions. The aerodynamics models considered are: stability derivatives, strip theory methods, quasi-steady vortex lattice methods, and unsteady panel methods. Through dynamic simulations using a virtual wind tunnel, differences between the various aerodynamics models are examined.

The simulations that were examined were primarily concerned with the short period mode in the longitudinal direction. Initial examinations were performed on single-surface geometries and showed good agreement between all models. The follow-up simulations of conventional- and canard-type aircraft configurations showed variations due primarily to the inclusion of a wake model for domain vorticity in the vortex lattice and unsteady panel methods. Although dynamics are considered, the simulations performed did not show unsteady aerodynamics effects causing significant differences in short-period responses. This suggests that the quasi-steady approaches traditionally considered are adequate for the majority of stability and control simulations. The use of unsteady panel methods is only required when reduced frequencies increase to the point where Theodorsens lag function contributes significantly to the aerodynamic behavior. This would be the case for high frequency forced flapping flight, but is generally not the case for aircraft.

Nomenclature

α	Angle of attack [rad]
a	Wing angle of incidence [deg]
AR	Aspect ratio
b	Wing span [m]
$\bar{c}$	Reference chord [m]
cl	Two-dimensional lift coefficient
CL_α	CL vs. α slope [1/deg]
CM_α	CM vs. α slope [1/deg]
$\mathbf{d}$	Distance from surface aerodynamic center to body (0,0,0) [m]
$\mathbf{d}_{CG}$	Distance from surface aerodynamic center to body CG [m]
dt	Timestep size [s]
ϵ	Oswald's coefficient[2]
$\mathbf{F}$	Force [N]

*Graduate Student, Department of Aeronautics and Astronautics, 77 Massachusetts Ave., Cambridge, MA 02139, AIAA Student Member.

†Professor, Department of Aeronautics and Astronautics, 77 Massachusetts Ave., Cambridge, MA 02139.

I_{YY}	Moment of inertia about body y axis [kg*m^2]
$\mathbf{M}$	Moment [M*m]
n_i	Multistep integrator step number
ω_b	Angular rate in body reference frame [rad/s]
θ_0	Initial pitch angle [deg]
$\mathbf{Q}_i$	Orientation quaternion in inertial reference frame
q	Pitch rate in body reference frame
$\mathbf{r}_i$	Body position in inertial reference frame [m]
ρ	Air density [kg/m^3]
t	Time [s]
$\bar{S}$	Reference surface area [m^2]
τ	CL correction factor[2]
$\mathbf{v}_i$	Body velocity in inertial reference frame [m/s]
$\mathbf{w}$	Wind vector ("from") [m/s]
$\mathbf{X}$	State vector for body or force model in dynamics engine
$\dot{\mathbf{X}}$	State derivatives vector for body or force model in dynamics engine

I. Introduction

Stability derivatives and other low fidelity models are frequently used in the design and flight simulation of aircraft. With the ability to routinely perform higher fidelity simulations of aircraft dynamics and maneuvers, the authors investigated several different fidelity models to determine the applicability of each and the impact of higher fidelity effects on the prediction of dynamic motion of aerodynamic bodies. The various drawbacks of the individual aerodynamics models considered are well-known;[3] however, the implications these drawbacks have on the simulation of flying bodies is less apparent. In this paper, traditional stability derivatives, strip theory, vortex lattice methods, and unsteady panel methods have been compared for three simple body geometries, and the applicability of each aerodynamics model is examined.

In order to investigate the various models a six degrees of freedom rigid body dynamics simulation tool has been developed. The tool was designed to allow easy integration with a variety of different aerodynamics models. The dynamics tool and the various models are described in detail in the paper.

The experiments considered in the paper focus, where feasible, on the differences in the models examined. The experiments started by examining single lifting surface models with a center of gravity (CG) position in front of the lifting surface. The center of gravity position and the moment of inertia about the geometry's pitch axis were varied in order to affect the damping and frequency of the short period oscillations. Attempts were made to adjust the model parameters so that the reduced frequency of the pitch oscillations reached the point where unsteady effects became noticeable in the simulation results. After the analysis of this basic geometry, an investigation into two-surface aircraft was performed. For this study, a conventional glider configuration and a canard configuration geometry were used. Studies of the short period mode of both of the aircraft were performed.

II. The Black Box Dynamics Engine

The authors used a six degrees of freedom (6-DOF) black box dynamics engine to solve the equations of motion for all simulations. This tool, created by one of the authors, is an application programming interface (API) written in the programming language C++; it allows users to define physical bodies with specified inertial properties and various types of forces and moments that act on those bodies. The tool is considered *black box* because creators of programs that use the API do not need to know the details of the API's method of equation-solving; they simply specify their body types and initial conditions, choose from a set of built-in force models (or plug in their own), and then select an integrator to march their simulations forward in time. The user can choose either a Forward Euler method or a fourth order Runge-Kutta method and specify a timestep size.

Several substates reside within each body's basic state vector, as shown in Equation 1:

$$\mathbf{X} = \begin{bmatrix} \mathbf{v}_i \\ \omega_b \\ \mathbf{Q}_i \\ \mathbf{r}_i \end{bmatrix} \tag{1}$$

where:

- $\mathbf{X}$ is the body's state vector
- $\mathbf{v}_i$ is the velocity in the inertial reference frame
- ω_b is the angular velocity in the body frame
- $\mathbf{Q}_i$ is a quaternion encoding the body's orientation in the inertial reference frame, as described in Wertz.[4] The engine uses quaternions to store body orientation to avoid singularities associated with storage methods that utilize Euler angles.
- $\mathbf{r}_i$ is the body's position in the inertial reference frame

The engine computes time derivatives of each body's state vector based on the body's current state and the forces and moments applied to it. The engine also computes time derivatives for force models that have their own state vectors. The general concept of this process is as seen in Equation (2):

$$\dot{\mathbf{X}} = f(\mathbf{X}, t, dt, n_i) \tag{2}$$

where:

- $\dot{\mathbf{X}}$ contains the derivatives of the state vector
- f represents the combined effects of anything that affects the state vector. For a body, this includes the sum of forces and moments applied by all force models (such as gravity, aerodynamic force, etc.). The dynamics engine provides a number of force models, including strip theory and stability derivatives aerodynamics models (described in Section III). Users of the dynamics engine can enhance the built-in models or provide new ones altogether by extending the engine's force model C++ classes.
- t is the current simulation time
- dt is the current timestep
- n_i is the current internal step number if a multistep integrator is used

A numerical integrator then creates the next states based on the derivatives and the user-specified timestep. Passing time, timestep, and internal step number information to the state function allows users of the dynamics engine to write time-dependent force models, such as unsteady aerodynamics models. After every iteration, users can access body states and information concerning applied forces and moments for display or archival purposes, and the dynamics engine contains a set of routines that can generate data files suitable for manipulation in MATLAB®.

Simulations using the dynamics engine conform to a basic execution format:

1. A physical body or a number of physical bodies is instantiated. The engine provides a generic rigid body model as well as rigid bodies containing information used by the strip theory and stability derivatives aerodynamics models (described in Section III), which were written concurrently with the dynamics engine.
2. The user specifies the initial conditions of each body.
3. The user instantiates force models and specifies which bodies they act upon; each body can receive forces and moments from multiple force models. Aerodynamics models typically take an atmosphere datatype as an input parameter; this division between aerodynamics model and atmosphere allows a user of the dynamics engine to easily change wind speed and air density (even during runtime) without the need to modify an aerodynamics model's source code.

4. The user adds the bodies and force models to a "universe" container, which represents a numerical integrator. The dynamics engine currently implements the Forward Euler and fourth order Runge-Kutta methods of integration.

5. Iterations of the simulation begin. In each iteration:

   (a) All bodies and force models update their state vectors; in the update process, force models read the states of bodies they affect and return forces and moments to the bodies. The bodies then return time derivatives of their states to the integrator. Time derivatives are also requested from force models that have state vectors.

   (b) The universe integrates all gathered time derivatives for each body and model and returns new states.

   (c) The user can record any state or derivative for postprocessing purposes.

A. The *windtunnel* Test Arena

The dynamics engine features an application named *windtunnel*, a virtual windtunnel that operates by fixing the test geometry's center of gravity in space and moving a virtual atmosphere around it. The tunnel has no gravity force. A user of the tunnel can specify the wind speed of the atmosphere in all three of the tunnel's inertial axes (Table 1). The user can also specify geometry initial conditions (orientation and angular rates) and unconstrain any of the three body axes so that the test geometry may rotate. This freedom makes the windtunnel a powerful tool for isolating and analyzing aircraft short-period modes. The authors used *windtunnel* for all of the primary analysis in this paper, and all simulations focused on the longitudinal behavior of the test geometries. Thus, only forces in the body x and z directions and moments about the body y axis were considered.

Table 1. Windtunnel coordinate system.

Axis	Description
1	Positive toward the front of the tunnel
2	Positive toward the right of the tunnel
3	Positive toward the bottom of the tunnel

B. The *fly* Test Arena

The dynamics engine also features an application named *fly*, a virtual world that allows the simulation of geometries in free flight. A user of this arena can specify the initial conditions of the simulated geometry as well as the wind speed of the atmosphere. Axis 3 of the tunnel aligns with the default gravity vector (of magnitude 9.81 m/s^2), but the user can specify an arbitrary magnitude and direction of gravity. The reference frame of the free flight test arena closely matches the frame of the virtual windtunnel, as seen in Table 2. Due to differences in aerodynamics models, simulation of unconstrained motion in *fly* leads to differing trajectories, making meaningful comparisons between models difficult. Thus, *fly* was not used in this investigation.

Table 2. Free flight arena coordinate system.

Axis	Description
1	Positive toward North
2	Positive toward East
3	Positive toward the bottom of the arena

III. Aerodynamics Models

A. The Strip Theory Aerodynamics Model

Strip theory, also known as blade element theory,[5] concerns dividing an aircraft's geometry into discrete segments and computing aerodynamic forces and moments on those segments based on their local velocities. Forces and moments are then summed across all segments to arrive at the total force on the aircraft's center of gravity (CG) and the total moment about it. This method of modeling an aircraft is general enough that users can specify main wings, stabilizer surfaces, and even rotary wings in a similar manner. Thus, aircraft designers can employ the strip theory flight model as a rapid development and behavioral estimation tool for a variety of aircraft geometries.

The strip theory model used by the authors allows the specification of each of an aircraft's flying surfaces in terms of angle of incidence, span, aspect ratio, location of aerodynamic center (assumed to be midway between the surface's tips at the quarter-chord position), number of segments, and other parameters. The strip theory file loader then discretizes each aircraft by breaking its surfaces into a number of rectangular chordwise segments of equal span. Each segment runs the entire chord length of its associated flying surface. Typical segment numbers ranged between 9 (for smaller stabilizer surfaces at low discretizations) and 21 (for main wing surfaces at high discretizations) for the simulations presented in this paper. The model currently implements rectangular wings, and symmetrical airfoils with no skin friction were assumed for the authors' investigation.

The strip theory model does not compute downwash and has no wake modeling. Instead, the model reduces the thin-airfoil theory cl vs. α slope of 2π based on the aspect ratio of each flying surface and a user-specified correction factor τ as described in Anderson[2] to approximate the CL for a three-dimensional finite wing. This CL and a user-specified Oswald's coefficient ϵ become inputs to an induced drag approximation.

During simulation, the strip theory model computes the total forces and moments on an aircraft using a number of steps for each of the aircraft's segments:

1. The model calculates the relative wind velocity at each segment's aerodynamic center based on the aircraft's linear CG velocity, angular velocity, and the wind velocity of the atmosphere at the location of the aerodynamic center.

2. The wind velocity and the segment orientation combine to give the local angle of attack and sideslip angle.

3. Using a simple approximation of a flat plate airfoil, the flight model computes the lift and drag coefficients for the segment. The model reduces the thin-airfoil theory cl vs. α slope of 2π based on the aspect ratio of the surface the segment belongs to as well as a user-specified value for τ. Segment CL, aspect ratio, and user-specified Oswald's efficiency coefficient ϵ become inputs to the induced drag calculation. The segment's coefficient of moment about the quarter-chord position is 0, in keeping with thin-airfoil theory.

4. Coefficients combine with local dynamic pressure (based on relative wind and atmosphere density) and segment surface area to produce lift and drag in a coordinate system aligned with the relative wind ("wind axes").

5. The model transforms the lift and drag to the body coordinate system to produce a body force. The body force vector and distance of the segment's aerodynamic center from the center of gravity combine to produce a body moment.

6. The model accumulates body forces and moments to arrive at the total applied force and moment from all of the aircraft's segments.

B. The Stability Derivatives Aerodynamics Model

The authors also employed a stability derivatives flight model based on the NPSNET simulation tool.[6] Each stability derivative represents the modeled aircraft's response to a small perturbation of a certain parameter; for example, the derivative $dCL/d\alpha$ describes how the aircraft's coefficient of lift changes given a small change in angle of attack α from a certain reference steady state value. The stability derivatives model

employed by the authors allows users to specify 26 aerodynamic parameters in total, including derivatives that account for unsteady behavior and wake effects. Users also specify a reference wing area, chord, and span.

During simulation, the stability derivatives model determines forces and moments on the modeled aircraft as follows:

1. The model computes the relative wind at the aircraft's center of gravity based on the aircraft's linear velocity and the atmospheric wind velocity at the CG. Relative wind velocity magnitude and atmospheric density combine to produce the dynamic pressure on the aircraft.

2. The model uses the relative wind velocity vector to compute the angle of attack and sideslip angle of the aircraft and generate a wind axes coordinate system based on both angles.

3. Angle of attack, sideslip angle, and dynamic pressure values join with force stability derivatives and reference parameters to produce lift, drag, and sideforce. The model transforms these forces into the body coordinate system to arrive at the total applied force on the aircraft's CG.

4. Aerodynamic states combine with moment stability derivatives and reference parameters to create the total roll, pitch, and yaw moments about the center of gravity.

C. The Vortex Lattice Method (VLM) Aerodynamics Model

The vortex lattice method[3] used by the authors resembles a basic quasi-steady membrane velocity boundary integral equation formulation for potential flow. The model represents the wing bound vorticity using a lattice of constant dipole panels, which are equivalent to vortex rings in a velocity formulation. The radiation condition is satisfied through the use of vortex ring elements, while the "no normal flow penetration through the mean surface" condition is satisfied through the solution of a linear system for the strengths of the vortex rings. In order to represent vorticity in the domain, the model utilizes a collection of vortex wake filaments in a wake sheet lattice. The wake sheet strength is prescribed by ensuring that a zero spanwise vorticity Kutta condition is satisfied at the trailing edge. Due to the necessity to automate simulations, the model extends the vortex wake behind the lifting surface to at least 40 chord lengths in the direction of the freestream velocity. This long wake ensures that the steady state lift will be achieved for the current state. Several variations of wake positions have been tested; across these variations, little overall change in the aerodynamic forces was observed.

The vortex lattice method computes forces and moments directly from the vortex strengths and the prescribed free stream velocity. As such, the induced drag is neglected in the computation of forces. The lack of induced drag plays a negligible role in most simulation results, and in situations where induced drag is important, variations in simulation results become apparent. Future work will consider implementing a Trefftz plane[3] analysis for the induced drag.

The vortex lattice method implemented for this investigation has known drawbacks which are consistent with vortex lattice methods in general. The usage of a simple quasi-steady flat sheet wake model is one source of error. Furthermore, the use of a low order ring vortex model causes slow force and moment values convergence when the panel discretization is increased. Additional errors manifest themselves due to the lack of body thickness. Errors which are thickness dependent, such as moment center position, moment and force values, and other finer details are neglected in the vortex lattice model. Although these effects are traditionally low order effects, mild changes in stability derivatives may lead to changes in the dynamic response.

D. The FastAero Panel Method Aerodynamics Model

The FastAero panel method[7] represents a novel approach for rapidly solving the unsteady potential flow around bodies with thickness. The method achieves rapid simulation times through the use of pFFT[8] and Fast Multipole Tree[9,10] matrix vector product acceleration approaches. The method implements a Green's theorem boundary integral equation formulation coupled with a vortex particle method representation of the unsteady vortex wake development. The use of a vortex particle method to describe the domain vorticity results in a method that is well suited to unsteady dynamic simulations due to the automatic convection of the vortex particles. With traditional panel method wake models, challenges commonly arise when the wake

surface interacts with downstream surfaces (such as a horizontal tail in the wash of a main wing). Using FastAero eliminates the concerns of vortex convection in the domain and provides a hands-off simulation environment in which high fidelity potential flow can be solved.

The version of FastAero used by the authors for this investigation differs from that described in Willis[7] in that it implements linear variations of doublet and source strengths over the surface panels. There are several advantages of using linear variations of the singularity strengths. First, the solution accuracy is improved over traditional constant collocation approaches due to the improved basis representation of the modeled boundary integral. The second advantage of linear basis implementations is the improved accuracy and ease in computing the surface velocities and pressures over surfaces meshed using triangles. This improved accuracy in computation of surface pressures leads to a more reliable computation of forces and moments, while the ability to use triangles in the discretization provides a means to efficiently mesh complex problems. Details of linear basis function implementations with accelerated methods can be found in Willis.[11]

FastAero is the only model of those considered that accounts for unsteady effects in the potential flow solution. Through the use of vortex particles in the wake, unsteady potential flow solutions are easily computed. Furthermore, FastAero considers high fidelity geometry representations which are not considered in any of the other models. Although the simulations presented in this investigation consider only lifting surfaces, it should be noted that the FastAero framework is capable of performing wing-body simulations. Simulations of full wing-body configurations would be expected to show some differences due to the inclusion of higher fidelity geometry representations. Finally, FastAero is capable of giving detailed surface pressure and domain velocity information. Although this is not of significant interest in the current investigation, the detailed loading information through flight maneuvers would likely be of interest to aircraft designers. Accounting for the higher fidelity solution effects comes at an increased computational cost.

IV. Test Geometries

A. Single Lifting Surface

Preliminary comparisons between the various aerodynamic models were performed using a single surface lifting body hinged about a prescribed forward CG position, described in the simulation reference frame shown in Table 3.

Table 3. Body coordinate system during simulations.

Axis	Description
x	Positive toward the front of the geometry
y	Positive toward the right of the geometry
z	Positive toward the bottom of the geometry

The lifting surface is analogous to an arrow with a horizontal fin and no vertical fin. If thrown in reality or modeled in *fly*, the body would follow a path similar to a ballistic trajectory. In the virtual windtunnel, however, the simplicity of the single lifting surface geometry makes it a useful tool for uncovering the differences between the aerodynamics models employed in this investigation. The geometry is presented in Figure 2(a), with properties shown in Table 4.

B. Conventional Glider

The conventional glider geometry represents a two-surface aircraft with a main wing and horizontal stabilizer behind it. It has the properties listed in Table 5 and the geometry visible in Figure 2(b).

C. Canard Glider

The canard glider geometry represents a two-surface aircraft with the main wing behind the horizontal stabilizer (called a canard in this configuration). The authors chose to model this aircraft with the hypothesis that the canard's wake covering the inboard section of the main wing would lead to more pronounced variations between the results of the various aerodynamics model employed in the investigation. The glider has the geometric properties listed in Table 6 and the geometry visible in Figure 2(c).

Table 4. Properties of the single lifting surface. d refers to the position of the aerodynamic center relative to (0,0,0) in the body reference frame.

Property	Value
Span	$b = 1.0$ m
Aspect Ratio	$AR = 6$
Angle of Incidence	$a = 0.0$ deg
x Position	$d_x = -1.0$ m
z Position	$d_z = 0.0$ m
Segments, Strip Theory	18
ϵ, Strip Theory	ϵ=0.8
τ, Strip Theory	τ=0.05
Panels, VLM	306
Panels, FastAero	1920

Table 5. Properties of the conventional glider.

Property	Value
Main Wing Span	$b_1 = 2.0$ m
Main Wing Aspect Ratio	$AR_1 = 18$
Main Wing Angle of Incidence	$a_1 = 3.0$ deg
Main Wing x Position	$d_{x_1} = -0.03$ m
Main Wing z Position	$d_{z_1} = 0.0$ m
Stabilizer Span	$b_2 = 0.6$ m
Stabilizer Aspect Ratio	$AR_2 = 6$
Stabilizer Angle of Incidence	$a_2 = 0.0$ deg
Stabilizer x Position	$d_{x_2} = -0.77$ m
Stabilizer z Position	$d_{z_2} = 0.0$ m
Total Segments, Strip Theory	315
ϵ_1, Strip Theory	$\epsilon_1 = 0.8$
τ_1, Strip Theory	$\tau_1 = 0.05$
ϵ_2, Strip Theory	$\epsilon_2 = 0.8$
τ_2, Strip Theory	$\tau_2 = 0.05$
Panels, VLM	612
Panels, FastAero	2816

Table 6. Properties of the canard glider.

Property	Value
Main Wing Span	$b_1 = 2.0$ m
Main Wing Aspect Ratio	$AR_1 = 10$
Main Wing Angle of Incidence	$a_1 = -0.5$ deg
Main Wing x Position	$r_{x_1} = -0.61$ m
Main Wing z Position	$r_{z_1} = 0.0$ m
Stabilizer Span	$b_2 = 0.6$ m
Stabilizer Aspect Ratio	$AR_2 = 8$
Stabilizer Angle of Incidence	$a_2 = 3.0$ deg
Stabilizer x Position	$r_{x_2} = 0.3$ m
Stabilizer z Position	$r_{z_2} = -0.15$ m
Total Segments, Strip Theory	315
ϵ_1, Strip Theory	$\epsilon_1 = 0.8$
τ_1, Strip Theory	$\tau_1 = 0.05$
ϵ_2, Strip Theory	$\epsilon_2 = 0.8$
τ_2, Strip Theory	$\tau_2 = 0.05$
Panels, VLM	612
Panels, FastAero	2816

The three geometries presented allowed the authors to perform a wide variety of tests with the aerodynamics models described in this investigation.

V. Results and Discussion

A. Convergence of the Pitch Rate

A pitch response convergence study was performed for both the time and spatial discretizations to illustrate the reliability of the analysis. Simulations of the single lifting surface were run in the virtual windtunnel using the input parameters shown in Table 7.

Table 7. Windtunnel and geometry initial conditions.

Parameter	Value
Timestep	$dt = 0.0025$ s
Wind From Axis 1	$w_1 = 30.0$ m/s
Wind From Axis 3	$w_3 = 0.0$ m/s
Air Density	$\rho = 1.225$ kg/m^3
Initial Pitch	$\theta_0 = 5.0$ deg

The spatial discretization convergence study illustrated in Figures 3(a)-3(c) was performed according to Table 8.

Figures 3(a) to 3(c) illustrate that the refinement of the discrete approximation of the wing has little effect on the pitch response. This demonstrates that both the regular and the refined discrete approximations will yield accurate results.

The dynamics engine can perform time integration using a fourth order Runge-Kutta scheme or a Forward Euler scheme. The convergence rates for the Forward Euler integration scheme are of particular interest due to the restrictions imposed by the internal integration scheme implemented in the current FastAero model. The convergence of the single lifting surface pitch response is considered for the different aerodynamics

Figure 1. Test geometries used in primary analysis.

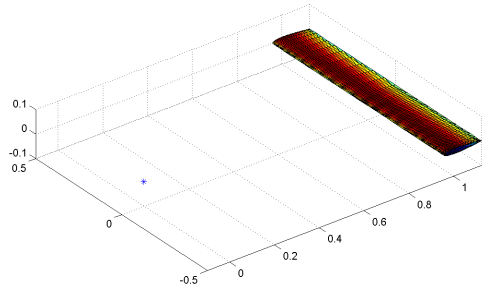

(a) The single lifting surface model considered as a testbed for the dynamic simulations. The "*" symbol indicates the CG position, which is one meter in front of the wing's aerodynamic center in the displayed geometry.

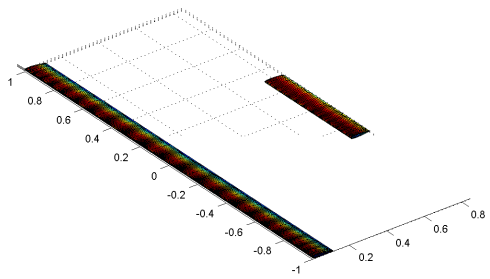

(b) The conventional glider geometry.

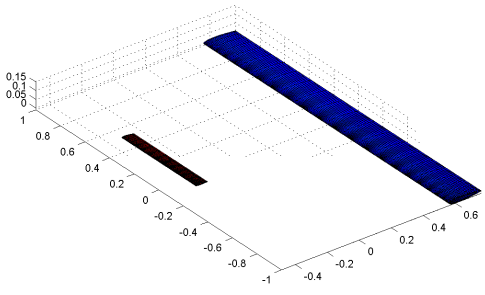

(c) The canard glider geometry.

Table 8. Number of elements in the single lifting surface discretization test.

Aerodynamics Model	Low	High
Strip Theory Segments	9	18
VLM Panels	144	306
FastAero Panels	640	1920

Figure 2. The pitch response considering the regular and fine discretization of the single lifting surface, $AR = 6$, $CG = -0.25$. All moments of inertia are of units [kg*m^2].

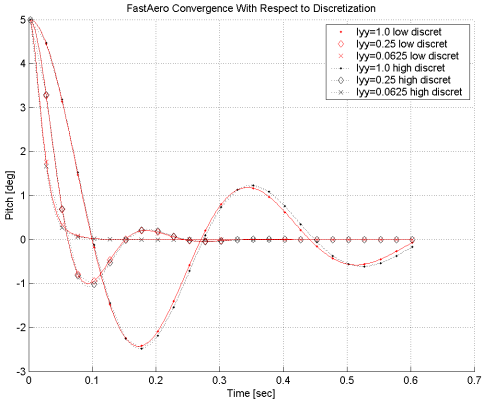

(a) FastAero convergence.

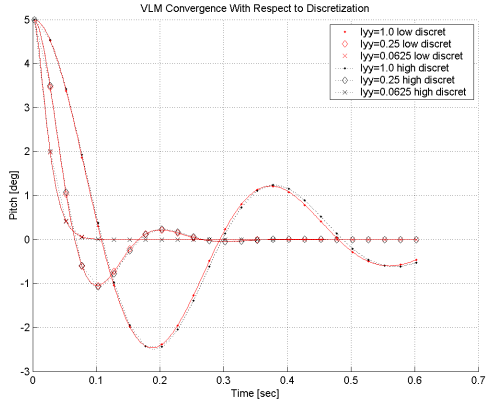

(b) VLM convergence.

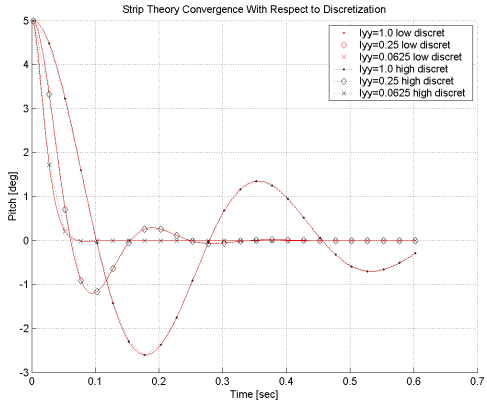

(c) Strip Theory convergence.

models and is illustrated in Figures 4(a) to 4(c), which demonstrate that the pitch response converges with reduced timestep as expected.

Figure 3. Timestep convergence behavior of the single lifting surface for the three aerodynamics models, $AR = 9$, $CG = 0.0$ m, $I_{YY} = 1.0$ kg*m^2.

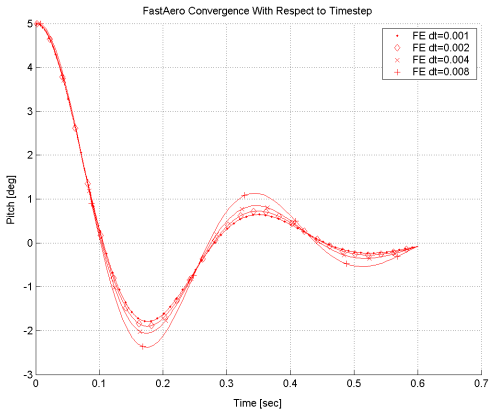

(a) FastAero convergence.

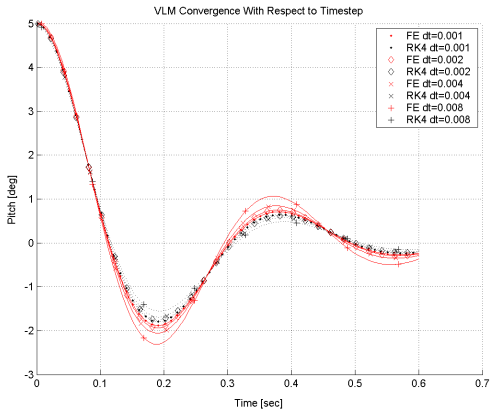

(b) VLM convergence.

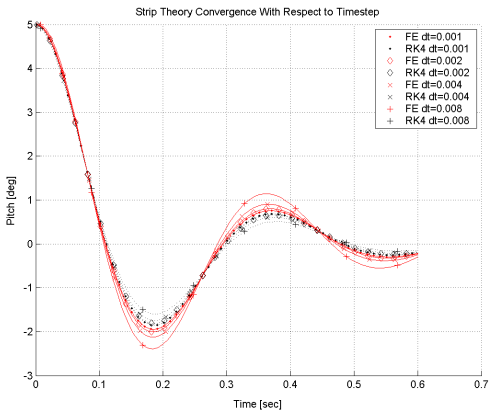

(c) Strip Theory convergence.

B. Single Lifting Surface Simulations

The simplicity of the single lifting surface makes it ideal for a range of simulations in the virtual windtunnel. Varying the x position of the body's center of gravity with respect to the aerodynamic center of the body's wing changes the geometry's pitch damping. Furthermore, varying the y axis moment of inertia I_{YY} changes the oscillation frequency of the surface. Through these simple parameter adjustments, it is possible to examine the trends between models in a controlled manner. Several sample pitch response plots are shown in Figures 5(a) to 5(d).

Due to the simplicity of the model, a comprehensive examination of the pitch frequency and overshoot amplitude trends was also performed. Figures 6(a) and 6(b) display the results of these simulations.

Upon considering the overshoot amplitude in Figure 6(b), it can be seen that in regions of faster response, the dynamics predicted using strip theory appears to tend away from the VLM and FastAero simulation results. This is due to wake downwash effects which are not modeled in the strip theory approach. In the dynamic response, this can be seen in Figure 5(d).

Figure 4. Pitch behavior of the single lifting surface.

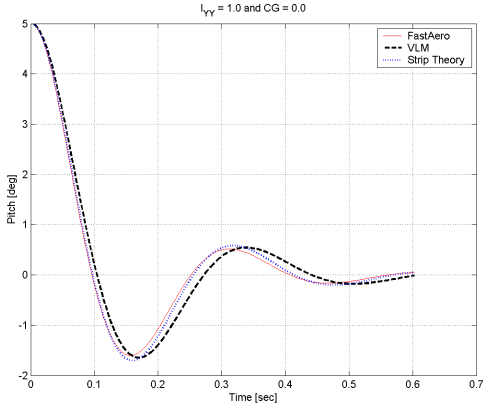

(a) $CG = 0.0$ m, $I_{YY} = 1.0$ kg*m^2.

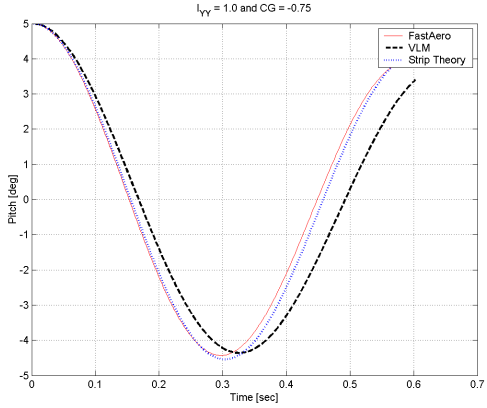

(b) $CG = -0.75$ m, $I_{YY} = 1.0$ kg*m^2.

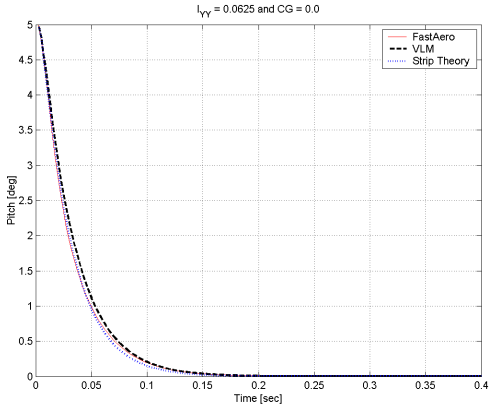

(c) $CG = 0.0$ m, $I_{YY} = 0.0625$ kg*m^2.

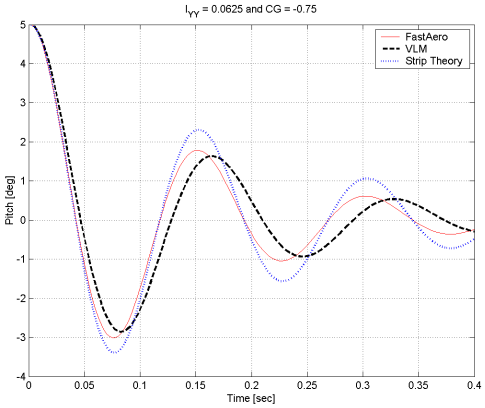

(d) $CG = -0.75$ m, $I_{YY} = 0.0625$ kg*m^2.

Figure 5. Pitch frequency and overshoot amplitude for the single lifting surface.

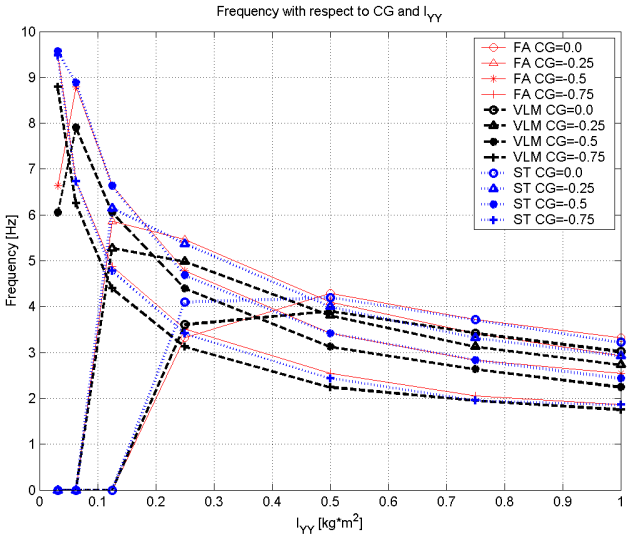

(a) Pitch frequency.

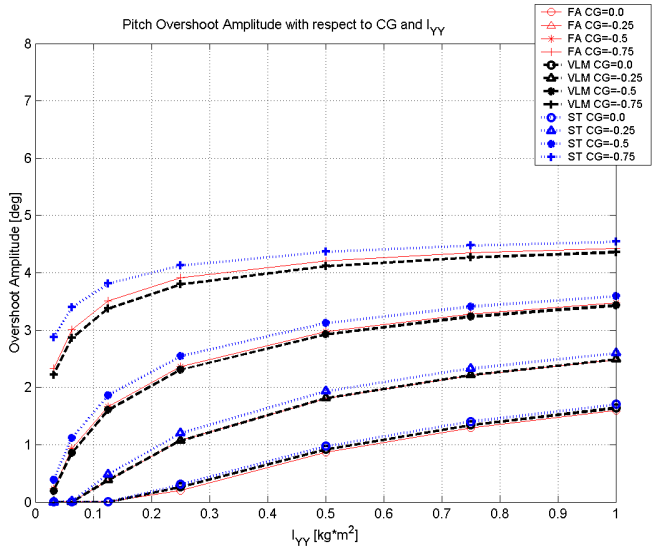

(b) Overshoot amplitude.

As a further analysis of the lifting surface's behavior under different aerodynamics models, stability derivatives of body z axis force and y axis moments were generated by reading the first data points of simulation results of the strip theory, VLM, and FastAero simulation results. These derivatives were compared with a set of stability derivatives generated by hand using Equations (3) to (8), based on Anderson[2] and McCormick.[12] The authors also employed hand (analytical) calculations for the pitch rate stability derivatives dF_z/dq and dM_y/dq, as seen in Equations (7) and (8). These are very difficult to obtain from simulation data, so they were not extracted from pitch curves given by the strip theory, vortex lattice method, or FastAero models. Note that the stability derivatives employed by the authors only relate to aerodynamic forces; thus, they do not change with changes in geometry mass or moment of inertia.

$$CL_\alpha = 2\pi \frac{1}{1 + \frac{2}{AR}(1+\tau)} \tag{3}$$

$$CM_\alpha = -CL_\alpha r_{CG}/\bar{c} \tag{4}$$

$$dF_z/d\alpha = -\frac{1}{2}\rho |v_i|^2 \bar{S} CL_\alpha \tag{5}$$

$$dM_y/d\alpha = \frac{1}{2}\rho |v_i|^2 \bar{S}\bar{c} CM_\alpha \tag{6}$$

$$dF_z/dq = -\frac{1}{2}\rho v CL_\alpha \bar{S} d_{CG} \tag{7}$$

$$dM_y/dq = d_{CG} dF_z/dq \tag{8}$$

Figures 7(a) and 7(b) show a comparison of angle of attack stability derivatives for the single lifting surface geometry. Figures 8(a) and 8(b) show hand-calculated pitch rate stability derivatives.

Figures 9(a)-9(d) display a comparison of pitch responses using FastAero, stability derivatives, and stability derivatives without rates. The stability derivatives curves were generated using the virtual windtunnel and the same initial conditions listed in Table 7. As seen in the figures, hand-calculated stability derivatives for the single lifting surface provide results that match well with the FastAero pitch results.

C. Discussion of the Single Lifting Surface Results

The results of the single lifting surface simulations demonstrate a close match between the various simulation models across all ranges of parameters considered. The short period mode in traditional aircraft is a heavily damped mode and occurs rapidly (if it contains frequency components they are typically high). In the series of simulations performed, the reduced frequency of motion is sufficiently small such that unsteady aerodynamic effects are not influential. Traditional stability and control analysis[12] assumes that aircraft will travel at least fifty chord lengths per oscillation; this situation is well approximated by quasi-steady theory and models. The assumption of quasi-steady flow in stability analysis of traditional aircraft is confirmed by the results. Although the FastAero model incorporates an unsteady wake, the approximations made in the development of the different aerodynamic models are sufficiently large compared with the small differences imposed by the higher fidelity wake modeling. If aeroelastic effects or flapping wings were considered, the reduced frequencies of the resulting motions would have an impact on the dynamic response.

D. Pitch Response of Aircraft Models

Although the single lifting surface study of the previous section presented a simple test case for the examination of the dynamic response trends, practical applications such as aircraft dynamic response will involve interactions between lifting and control surfaces which will further influence the dynamic response. The authors examined a conventional glider and a canard glider (described in Section IV) using the virtual wind tunnel under the conditions shown in Table 9. The results of these simulations are shown in Figures 10(a)-10(e).

E. Discussion of the Aircraft Results

The results from the aircraft simulations illustrate additional differences between the aerodynamic models considered. The aerodynamics models have different wake representations. In the strip theory analysis, wake

Figure 6. Comparisons of stability derivatives for the single lifting surface.

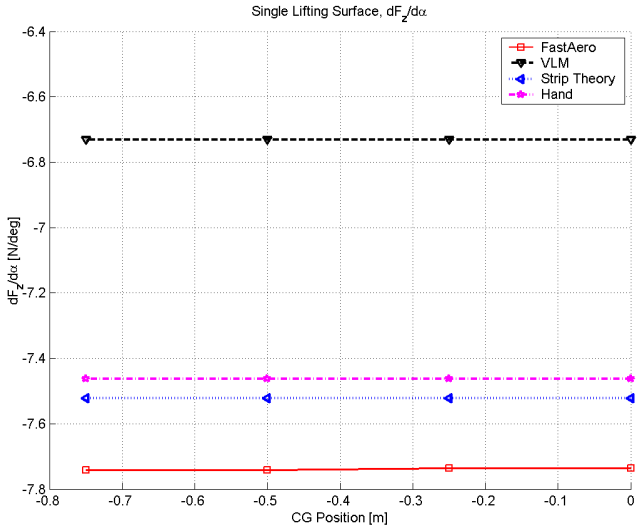

(a) $dF_z/d\alpha$.

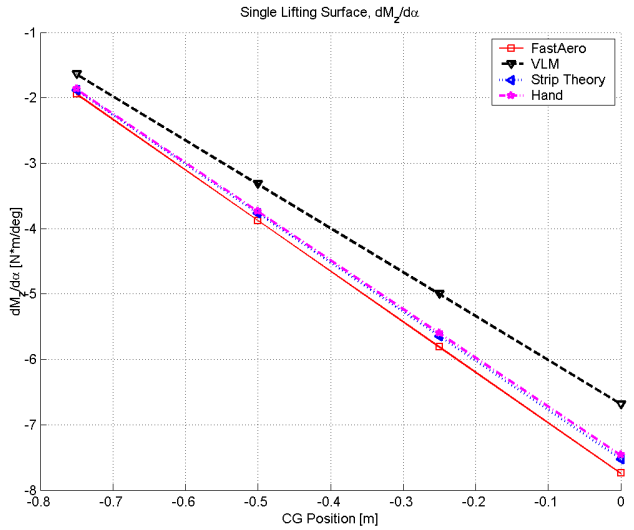

(b) $dM_y/d\alpha$.

Figure 7. Hand-calculated pitch rate stability derivatives.

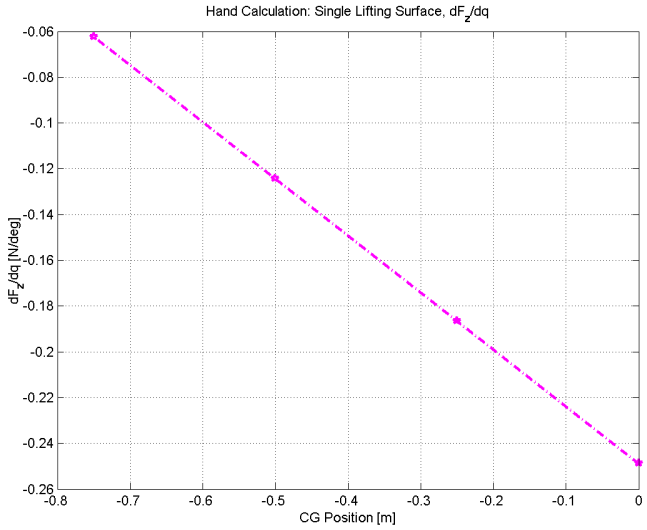

(a) dF_z/dq.

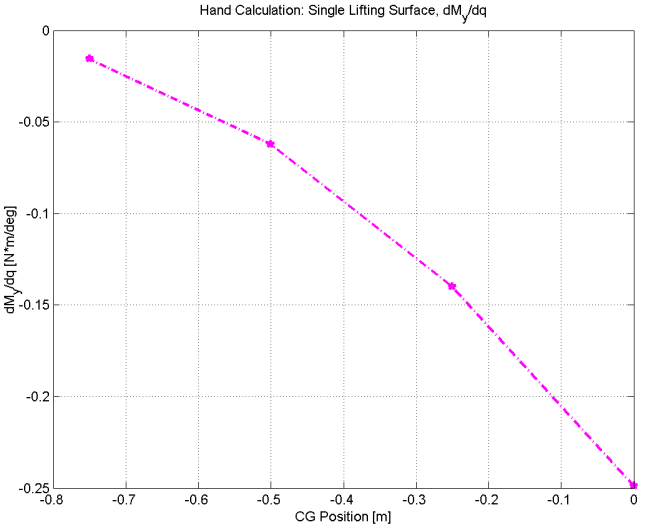

(b) dM_y/dq.

Figure 8. Comparisons between FastAero and stability derivatives models for the single lifting surface.

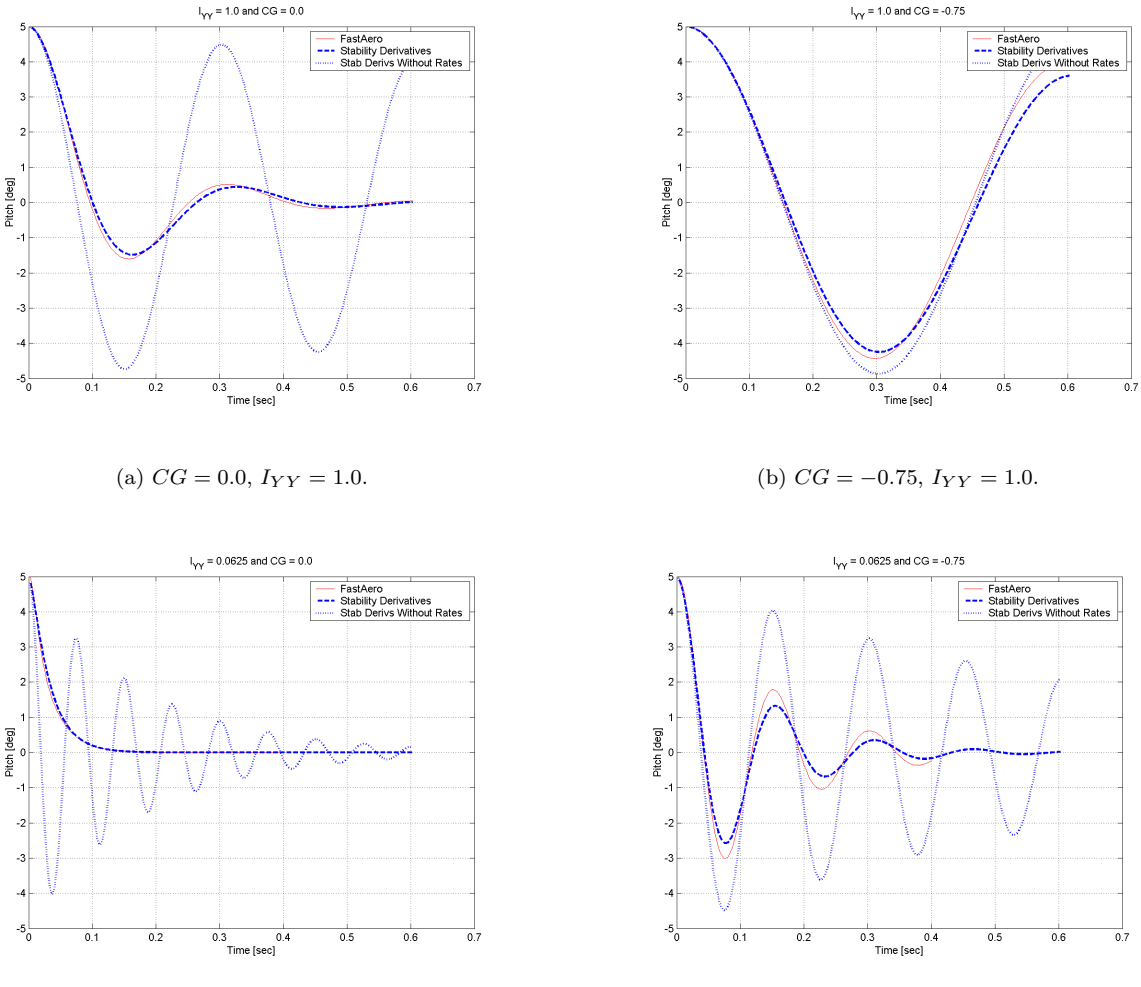

(a) $CG = 0.0$, $I_{YY} = 1.0$.

(b) $CG = -0.75$, $I_{YY} = 1.0$.

(c) $CG = 0.0$, $I_{YY} = 0.0625$.

(d) $CG = -0.75$, $I_{YY} = 0.0625$.

Table 9. Windtunnel and geometry initial conditions for aircraft.

Parameter	Value
Timestep	$dt = 0.0025$ s
Wind From Axis 1	$w_1 = 30.0$ m/s
Wind From Axis 3	$w_3 = 0.0$ m/s
Air Density	$\rho = 1.225$ kg/m^3
Initial Pitch, Conventional Glider	$\theta_0 = 5.0$ deg
Initial Pitch, Canard Glider	$\theta_0 = 1.0$ deg

Figure 9. Pitch behavior of the aircraft.

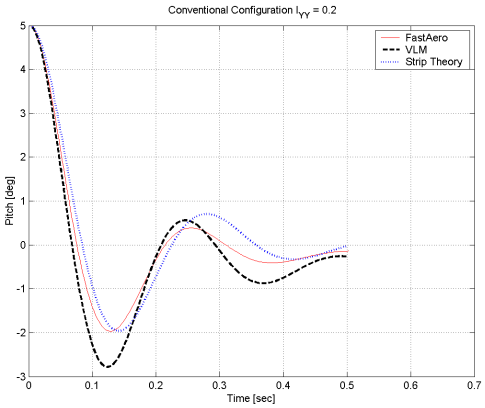

(a) Conventional glider, $I_{YY} = 0.2$.

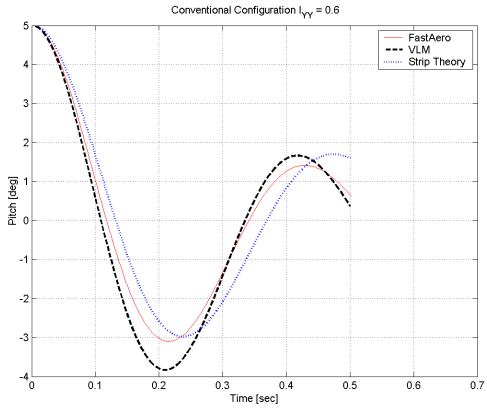

(b) Conventional glider, $I_{YY} = 0.6$.

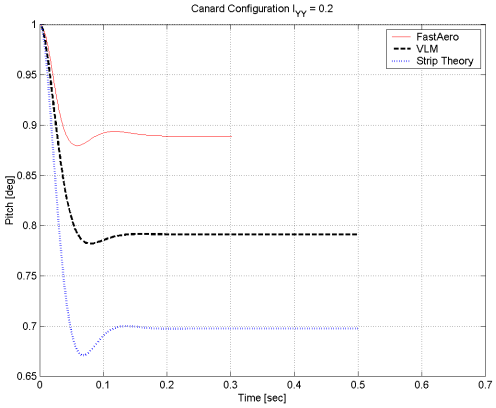

(c) Canard glider, $I_{YY} = 0.2$.

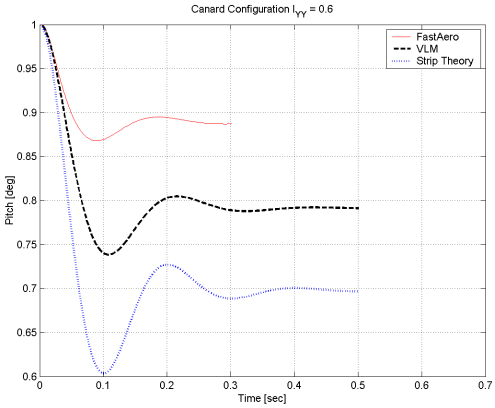

(d) Canard glider, $I_{YY} = 0.6$.

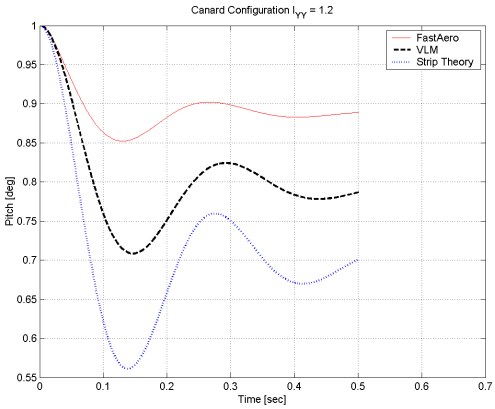

(e) Canard glider, $I_{YY} = 1.2$.

downwash is not approximated. In the vortex lattice method the wake is represented using rigid filaments of vorticity oriented in the free stream flow direction. The FastAero wake modeling involves discrete vortex particles which advect under the influence of the local flow, and stretch according to local gradients in the flow. From Figures 10(c)-10(e), it can be seen that the steady state pitch is different between the models by a fraction of a degree. The strip theory has the lowest steady state pitch angle of the three models, and this is assumed to be due to the lack of any canard wake downwash on the main wing. The VLM and FastAero both require the canard model to have a higher pitch angle to compensate from lift lost over the main wing due to canard wake downwash. The differences between the steady state pitch in these two models are likely due to several factors, namely the VLM having a prescribed wake position and the various physical modeling differences between the two approximations. Although the steady state pitch angle is different, the results demonstrate the models predict the dynamic response comparably. Similarly, with the conventional aircraft configuration, the results show good agreement across the different aerodynamic models.

VI. Conclusion

The general 6-DOF simulation tool for the simulation of rigid body dynamics was successfully coupled with several different fidelity aerodynamics models. The aerodynamics models considered were a stability derivative model, a strip theory model, a vortex lattice model and an unsteady panel method. The results of the dynamic simulations across a range of parameters showed good agreement between the models which suggests that the various force models are relatively interchangeable in the analysis of dynamic response. Differences in dynamic response exist when the domain vorticity is not accurately modeled on downstream lifting surfaces; however, little effect was perceived with regard to unsteady aerodynamics due to the relatively low reduced frequency of the simulations. The use of higher fidelity models such as VLM and FastAero would be beneficial in the situations where more detailed information is desired, such as surface loading. It should be noted that when the aircraft fuselage and appendages are considered in the models capable of that analysis, more radical differences between the low and higher fidelity models will be found.

Acknowledgements

The authors would like to acknowledge the support for the investigation and related research provided by the R.L. Bisplinghoff Fellowship, MIT's Department of Aeronautics and Astronautics, the Natural Sciences and Engineering Research Council of Canada (NSERC), the Singapore-MIT Alliance (SMA), and the National Science Foundation (NSF).

References

[1]Etkin, B. and Reid, L. D., *Dynamics of Flight: Stability and Control*, John Wiley and Sons, 3rd ed., 2000.

[2]Anderson Jr., J. D., *Fundamentals of Aerodynamics*, McGraw-Hill, 3rd ed., 2001.

[3]Katz, J. and Plotkin, A., *Low-Speed Aerodynamics*, Cambridge University Press, 2nd ed., 2000.

[4]Wertz, J. R., *Spacecraft Attitude Determination and Control*, Springer, 1st ed., 1978.

[5]Weick, F. E., "Propeller Design, Practical Application of the Blade Element Theory - I," Tech. Rep. TR235, National Advisory Committee for Aeronautics, 1994.

[6]Cooke, J. M., Zyda, M. J., Pratt, D. R., and McGhee, R. B., "NPSNET: Flight Simulation Dynamic Modeling Using Quaternions," *Presence*, Vol. 1, No. 4, 1994, pp. 404–420.

[7]Willis, D. J., Peraire, J., and White, J. K., "A Combined pFFT-Multipole Tree Code, Unsteady Panel Method With Vortex Particle Wakes," Aiaa paper 2005–0854, American Institute of Aeronautics and Astronautics, Reno, NV, USA, Jan. 2005.

[8]Philips, R. and White, J. K., "A Precorrected-FFT Method for Electrostatic Analysis of Complicated 3-D Structures," *IEEE Transactions on Computer-Aided Design of Integrated Circuits*, Vol. 16, 1997.

[9]Greengard, L. and Rohklin, V., "A Fast Algorithm for Particle Simulations," *Journal of Computational Physics*, Vol. 73, 1987, pp. 325–384.

[10]Barnes, J. and Hut, P., "A Hierarchical O(N log N) Force Caluclation Algorithm," *Nature*, Vol. 324, 1986, pp. 446–449.

[11]Willis, D. J., White, J. K., and Peraire, J., "A pFFT Accelerated Linear Strength BEM Potential Solver," *7th International Conference on Modeling & Simulation of Microsystems*, Boston, MA, USA, March 2004.

[12]McCormick, B. W., *Aerodynamics, Aeronautics, and Flight Mechanics*, Wiley, 2nd ed., Aug. 1994.